Effect of Re Addition on Microstructure and Oxidation Resistance of Co-Cr-Ta-Ti-C Alloys

Louis Etienne Moreau , Santhosh Banoth , Akira Ishida , Hideyuki Murakami *

Posted Date: 17 November 2023

doi: 10.20944/preprints202311.1123.v1

Keywords: Co-Cr alloys; phase constitution; differential thermal analysis; Calphad simulation; high temperature oxidation

Article

Effect of Re Addition on Microstructure and Oxidation Resistance of Co-Cr-Ta-Ti-C Alloys

Louis Etienne Moreau [1,2], Santhosh Banoth [2,3], Akira Ishida [2] and Hideyuki Murakami [1,2,*]

[1] Department of Nanoscience and Nanoengineering, Waseda University, 3-4-1 Okubo, Shinjuku, Tokyo 169-8555, Japan
[2] Research Center for Structural Materials, National Institute for Materials Science, 1-2-1 Sengen, Tsukuba, Ibaraki, 305-0047, Japan
3 Department of Mechanical Systems Engineering, Tokyo Metropolitan University, 1-1, Hachioj, Tokyo 192-0397, Japan
* Correspondence: murakami.hideyuki@nims.go.jp; Tel.: +81-29-859-2560

Abstract: This study investigates the effect of Re addition on the microstructure evolution and oxidation resistance of Co-Cr-Ta-Ti-C alloys. The alloys tested in this study consist of a Co-rich matrix with mixed HCP and FCC phases, together with $TaTiC_2$ and Ti-based carbides. The addition of Re promotes the precipitation and growth of a CoCr-rich σ phase. Differential thermal analysis (DTA) showed that the melting temperatures did not change drastically up to 10 at% Re addition, whereas 15 at% Re addition significantly increased the melting temperature of the alloys. Oxidation tests in air at 1200°C showed that excessive Re content could lead to deterioration in oxidation resistance, mainly due to the accelerated formation of volatile Re oxides.

Keywords: Co-Cr alloys; phase constitution; differential thermal analysis; Calphad simulation; high temperature oxidation

1. Introduction

Improved high-temperature materials development is in demand from gas turbines to increase inlet gas temperatures, improve energy efficiency and reduce CO_2 emissions [1]. Currently, Ni-based and Co-based superalloys are the primary materials used in the hottest sections of gas turbines [2–6]. In the Ni-based or Co-based superalloys, the $L1_2$-structured Ni_3Al or Co_3Al-based precipitates principally improve their mechanical properties. Alloying addition of Al also effectively enhances their oxidation resistance by forming the stable Al_2O_3 layer on their surfaces. However, the temperature capabilities of superalloys are limited by the ability to raise the melting point of the alloys, which is in turn determined by the melting temperature of its main constituent Ni (1453°C) and Co (1495°C). In addition, for some high-temperature applications such as glass industries, the formation of Al_2O_3 or SiO_2 should be avoided because they could dissolve into the liquid glass, which results in the contamination of the raw material.

Under such circumstances, Co-Cr-based alloys are focused. Berthod et al. proposed Co-Cr-Ta-C alloys having reasonable mechanical properties at high temperatures [7,8]. In this alloy system, Cr_2O_3 is formed on the alloy surface. While Cr_2O_3 remains stable up to 1000°C, it rapidly loses its protective properties at higher temperatures due to its favored transformation into gaseous CrO_3 [9–13]. Recently, we confirmed that in the Co-Cr-Ta alloy system, the formation of $CrTaO_4$ effectively keeps its protective properties at 1200°C. However, since the melting points of this alloy system are predicted to be 1200 to 1400°C [14], we need further alloy design to increase the melting point, given they are used at temperatures above 1000°C.

 doi:10.20944/preprints202311.1123.v1

To increase the melting temperature of alloys, the addition of the refractory element of Re (3182°C) is promising. Re readily dissolves into Co and forms a continuous solid solution system. Thus, the melting temperatures of Co-Re-based alloys with specific strength are much higher than those in Ni-based superalloys [15,16]. Superalloys used in gas turbines also need good mechanical properties at elevated temperatures [17], which can be achieved by adding Re [18,19]. Investigation of the Co-Cr-Re-Ta-C alloy system has also been conducted for the next-generation materials at high temperatures [20], with the formation of stable monocarbides observed at 1200°C.

On the other hand, previous research [21] has shown that Co-Re binary alloys have poor oxidation resistance due to the formation of a porous and non-protective Co-oxide layer, leading to significant loss of Re through the formation of volatile ReO_3 [20,21]. To improve the oxidation behavior, it is necessary to add sufficient Cr content (>25 at%) to the Co-Re alloy to form Cr_2O_3 [22,23], which retards the evaporation of Re oxides and provides protection against severe oxidation at high temperatures, or possible formation of $CrTaO_4$ could protect Co-Re-based alloys against oxidation [14].

The present study discusses the effect of Re addition on the microstructure and oxidation resistance of the Co-Cr-Ta-Ti-C alloy system. The alloy system is strengthened by the formation of Ti and Ta carbides [24,25], having a reasonable combination of mechanical properties and oxidation resistance at high temperatures. Since the alloys do not contain Al or Si, they have been applied as components for glass fiber fabrication [24,25].

Four alloys with different Re content (ranging from 0 at% to 15 at%) were characterized. The microstructural characterization, changes in phase constitution, melting temperature, and growth kinetics of the oxide layers at 1200°C were investigated as a function of Re content.

2. Experimental Procedures

The compositions of alloys investigated in this study are listed in **Table 1**. Cobalt was chosen as the primary component due to its high-temperature performance, chromium was added for improved oxidation resistance, and titanium and tantalum were added to strengthen the alloys by forming (Ta, Ti) carbides, respectively. The composition of Re-0 was determined from the literature [7,8]. Rhenium was included in the range of 0-15 at% to examine its effect on microstructure and oxidation kinetics. The alloys were fabricated using the arc melting method, where a mixture of source elements with a purity of higher than 99.9% was placed in a water-cooled copper mold and melted to form approximately 15 g of alloy buttons. These buttons were then sealed in quartz ampoules under argon and heat-treated at 1200°C in a box furnace (SANSYO, MSFT-1520) followed by air-cooling to homogenize the samples.

Table 1. Composition of alloys investigated in this study.

Alloys	Co (at.%)	Cr (at.%)	Re (at. %)	Ta (at. %)	Ti (at.%)	C (at.%)
Re-0	58.8	27		1.7	6.4	6.1
Re-5	53.8	27	5	1.7	6.4	6.1
Re-10	48.8	27	10	1.7	6.4	6.1
Re-15	43.8	27	15	1.7	6.4	6.1

Phase identification was conducted by X-ray diffractometry (XRD) (MINIFLEX, Rigaku). Microstructure observation and the local chemical analysis of the specimens prior to the oxidation tests were carried out using scanning electron microscopy with energy dispersive spectroscopy (SEM-EDS) (JSM-7200F, JEOL), respectively. In the XRD analysis, the Cr Kα X-ray (λ = 2.2909 Å) target was used, with the scanning angle (2θ) ranging from 30 to 140°. After screening the possible phases using the Smartlab Studio II software, they were confirmed by comparing the interplanar distance

 doi:10.20944/preprints202311.1123.v1

(*dhkl*) calculated from the diffraction patterns with those from the International Centre for Diffraction Data (ICDD) cards of the highest quality [26]. From the set of d values, the crystal structure and the lattice parameter a (Å) of a specific phase were identified using codes such as $d_{hkl} = \frac{a}{\sqrt{h^2+k^2+l^2}}$ for a cubic phase and $d_{hkl} = \frac{a}{\sqrt{h^2+k^2+\frac{a^2}{c^2}l^2}}$ for a tetragonal phase for a given (hkl) crystal orientation. For microstructure and local chemical analysis, the backscattered electron (BSE) mode was mainly used. Samples were first mounted using conductive resin (Polyfast), heated at 180°C for 3 minutes, and cooled for 2 minutes. They were then polished using Emery paper up to 400 grit (38 μm), followed by the Metadi supreme Polycrystalline Diamond suspension up to 1 μm, and finished with a Chemomet cloth and Mastermet colloidal silica polishing suspension etching (up to 0.5 μm). The composition of each phase was averaged over at least twenty measurements using EDS.

The melting temperatures for each alloy composition were measured using differential thermal analysis (DTA) (Labsys, Setaram) [27]. DTA samples were cut into small cylinders with a diameter of approximately φ3 mm. They were then heated from room temperature to 1550°C and cooled at a heating/cooling rate of 10°C/min in a flowing Ar atmosphere. To characterize the microstructure changes of the alloys after oxidation, small pieces of samples were oxidized in a muffle furnace at 1200°C in the air for 20 h. The samples were placed on an Al_2O_3 plate, which was then slid into the furnace after it reached the target temperature. After 20 h of oxidation, the samples were removed from the furnace and air-cooled to room temperature. The sample mass changes were measured by weighing the samples, excluding spalled oxides.

The phase constitutions of the Co-Cr-Re-Ta-Ti-C alloy system as a function of temperature were predicted using Pandat 2020 software with PanNi2020 database, which included all the elements available in the present study, was applied for the thermodynamic predictions.

3. Results and Discussions

3.1. Microstructure of the alloys

The X-ray diffraction patterns of the arc-melted Co-Cr-Re-Ta-Ti-C alloys after annealing at 1200°C for 24 hours and air cooling are shown in **Figure 1**. All the alloys have three face-centered cubic (FCC) phases and one hexagonal close-packed (HCP) phase. A tetragonal phase is also detected in alloys Re-10 and Re-15. **Figure 2** provides BSE images of the microstructures, and **Table 2** summarizes the corresponding EDS analysis results, respectively. All the cast alloys exhibit dendritic microstructures after annealing at 1200°C. The microstructure of alloys Re-0 and Re-5 **(Figures 2(a), (b), (e), (f)**) consists of two Co-rich phases (darker region) forming the matrix of the alloy, large star-shaped (Ta, Ti)-rich carbides (grey region), and Ti-rich carbides (black region). The shape of the (Ta, Ti)-rich carbides appears to be due to the agglomerate of several carbides, and the size of the carbides decreases as the Re content increases. More isolated carbides are observed in Re-5. In alloys Re-10 and Re-15, the distribution of the carbides changes so that they are arranged in a row. Also, increasing the Re content from Re-5 to Re-15 (**Figures 2(b)-(d), (f)-(h)**) causes a decrease in the volume fraction of Co FCC and HCP phases and the formation of an additional CoCr-rich tetragonal phase. Through XRD, EDS, and BSE characterization, the matrix of the material was identified as a mixture of Co (HCP) and Co (FCC) phases. (Ta, Ti)-rich carbides were identified as $TaTiC_2$ (FCC, a=4.387Å) with the observed presence of TiC (FCC, 4.328 Å) alone. The tetragonal phase present in the Re-10 and Re-15 alloys was identified as the CoCr-rich sigma phase.

Preprints (www.preprints.org) | NOT PEER-REVIEWED | Posted: 17 November 2023 doi:10.20944/preprints202311.1123.v1

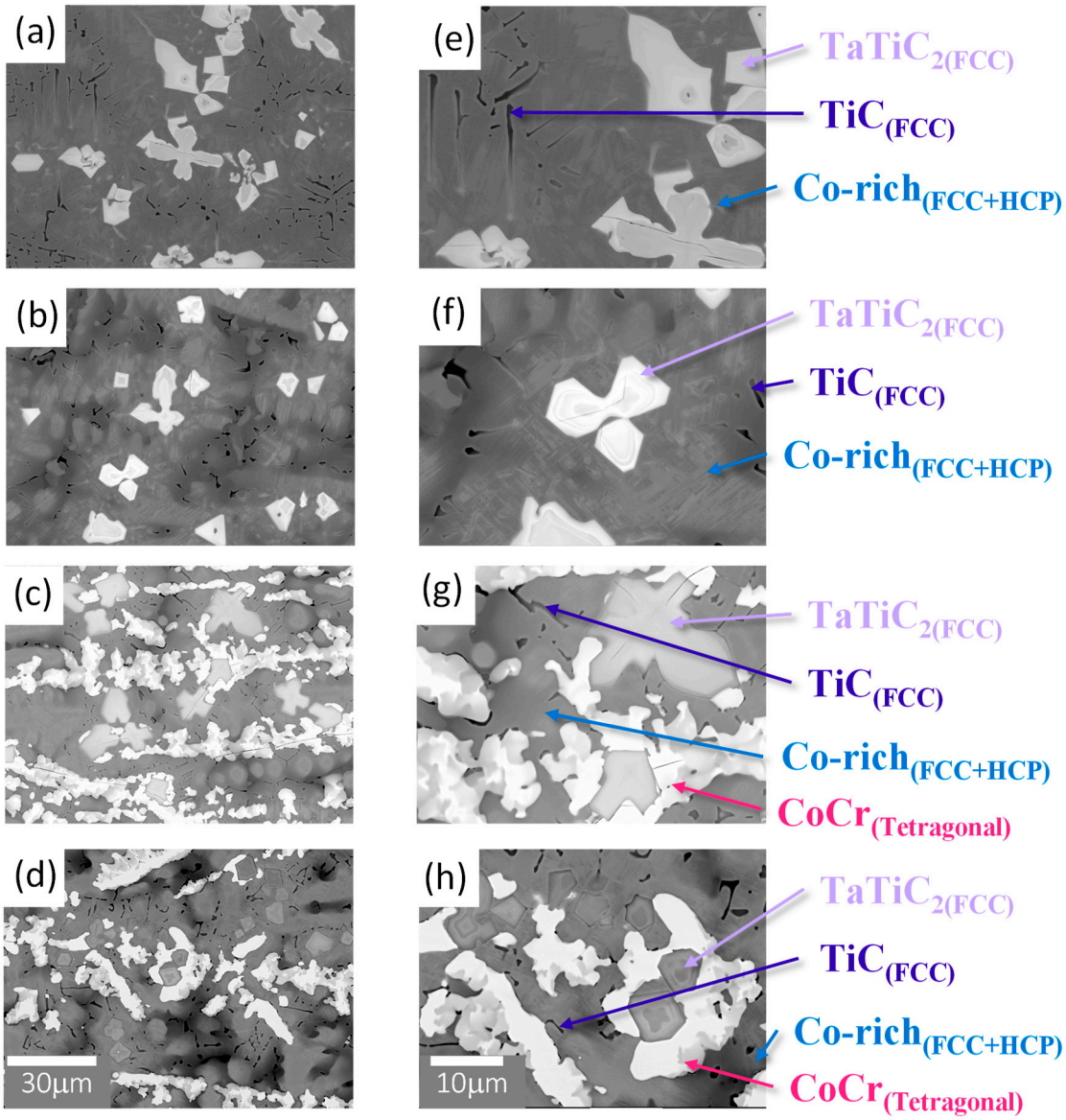

Figure 2. BSE images of studied alloys prepared by arc-melting followed by annealing at 1200°C for 24 hours: Low magnification images show the dendritic microstructure, and higher-magnification images give details of the carbides and the sigma phase.

Table 2. Composition of the phase observed in the studied Co-Cr-Ta alloys prepared by arc-melting followed by annealing at 1200°C for 24 hours (in at%).

Phases	Co	Cr	Re	Ta	Ti	C
Re-0	**58.8**	**27**	**0**	**1.7**	**6.4**	**6.1**
Dark grey region (HCP+FCC)	64.1	26.6	/	0.04	1.9	4.6
Black region (TiC)	28.7	15.7	/	4.5	29.3	21.9
Light grey region ($TaTiC_2$)	2.1	4.0	/	19.6	47.1	27.1
Re-5	**53.8**	**27**	**5**	**1.7**	**6.4**	**6.1**
Dark grey region (HCP+FCC)	60.1	27.8	2.8	0.3	3.2	5.7
Black region (TiC)	18.5	10.9	0.4	9.7	38.9	21.9
Light grey region ($TaTiC_2$)	2.5	1.6	/	27.7	41.1	27.1

 doi:10.20944/preprints202311.1123.v1

Re-10	**48.8**	**27**	**10**	**1.7**	**6.4**	**6.1**
Dark grey region (HCP+FCC)	61.8	24.3	4.4	0.3	2.6	6.6
Black region (TiC)	23.8	13.9	2.4	8.4	29.2	22.4
Light grey region ($TaTiC_2$)	3.9	2.5	/	22.3	44.2	27.0
White region (s phase)	42.4	31.7	10.6	1.4	6.2	7.6
Re-15	**43.8**	**27**	**15**	**1.7**	**6.4**	**6.1**
Dark grey region (HCP+FCC)	62.4	21.1	8.7	0.3	1.4	6.0
Black region (TiC)	19.1	9.5	2.8	8.3	35.8	24.5
Light grey region ($TaTiC_2$)	1.8	1.5	/	24.8	44.7	27.1
White region (s phase)	39.2	29.5	20.8	0.8	2.4	7.2

The experimental results for the microstructure and the composition of each phase in the Co-Cr-Re-Ta-Ti-C alloys were compared with the thermodynamic phase simulation, as shown in **Figure 3**. The predicted phase compositions at 1200°C generally agreed with the experimental results, although there were some differences. The alloys Re-0 and Re-5 were mainly composed of the FCC phase with an additional FCC-MC phase. The main FCC phase is likely to correspond to the Co-rich FCC phase, and the FCC-MC2 corresponds to the $TaTiC_2$ (FCC) phase.

On the other hand, the HCP phase observed in all the alloys, as shown in **Figure 2** and **Table 2**, does not appear in the predicted phase diagrams for Re-0 and Re-5 at 1200°C. From the simulations, this phase is predicted to form at 898.2°C for Re-0 and at 1045.3°C for Re-5, respectively. Therefore, the formation of the HCP phase in Re-0 and Re-5 may have occurred during the air-cooling process after the heat treatment, which could explain its presence confirmed by the microstructural characterization as well as its predicted formation at lower temperatures. The presence of the ◎ phase was also expected for Re-10 and Re-15, corresponding to the observed CoCr-rich **σ** phase (tetragonal). The volume fraction of the **σ** phase is expected to increase significantly with the addition of Re, reaching around 10% in the alloy Re-15, which corresponds to the observations on the BSE images (**Figures 2(c), (d), (g), (h)**). According to the phase predictions, the volume fraction of $TaTiC_2$ remained constant across the range of alloys from Re-0 to Re-15. This finding is consistent with the microstructural observations made using the BSE mode (**Figure 2**). However, in the predictions, it was found that increasing the Re content of the alloys increases the temperature at which the Co-rich FCC phase forms and decreases the volume fraction of the HCP phase. Further observations are needed to confirm the trend of phase formation with temperature in the Co-Cr-Re-Ta-Ti-C system. It should be noted that the thermodynamic database (PanNi-2020) used in this study is optimized for Ni-based alloys. Nevertheless, these results appear to be consistent with observations for samples heat treated at 1200°C, and predictive tools such as Pandat show promise for optimizing the composition and microstructure of complex alloys in the future.

3.2. Evolution of melting temperatures

In addition to predicting equilibrium phase compositions as a function of temperature, the diagrams also provide information on the temperatures at which phase transformations occur. Therefore, the calculation of phase diagram software can be used to estimate the melting temperatures of Co-Cr-Ta-Ti-C alloys. From the calculation shown in **Figure 3**, the solidus temperature decreases slightly with increasing Re addition up to 10 at%; 1334.1°C for Re-0, 1324.8°C for Re-5 and 1321.2°C for Re-10, respectively. Then the 15 at% Re addition is predicted to drastically reduce the solidus temperature to 1255.9°C.

Figure 4 shows the DTA heat flow curves of the Co-Cr-Re-Ta-Ti-C alloys obtained from (a) the heating phase from room temperature to 1550°C and (b) the cooling phase from 1550°C to room temperature, respectively. As the sample temperature rises and melting starts, the temperature rise

Preprints (www.preprints.org) | NOT PEER-REVIEWED | Posted: 17 November 2023 doi:10.20944/preprints202311.1123.v1

of the sample stops and the heat flow from the reference to the sample increases. Therefore, the endothermic reaction of the sample, such as melting, is shown as a negative slope in the heat flow curve. When melting stops, the heat flow curve quickly returns to the baseline.

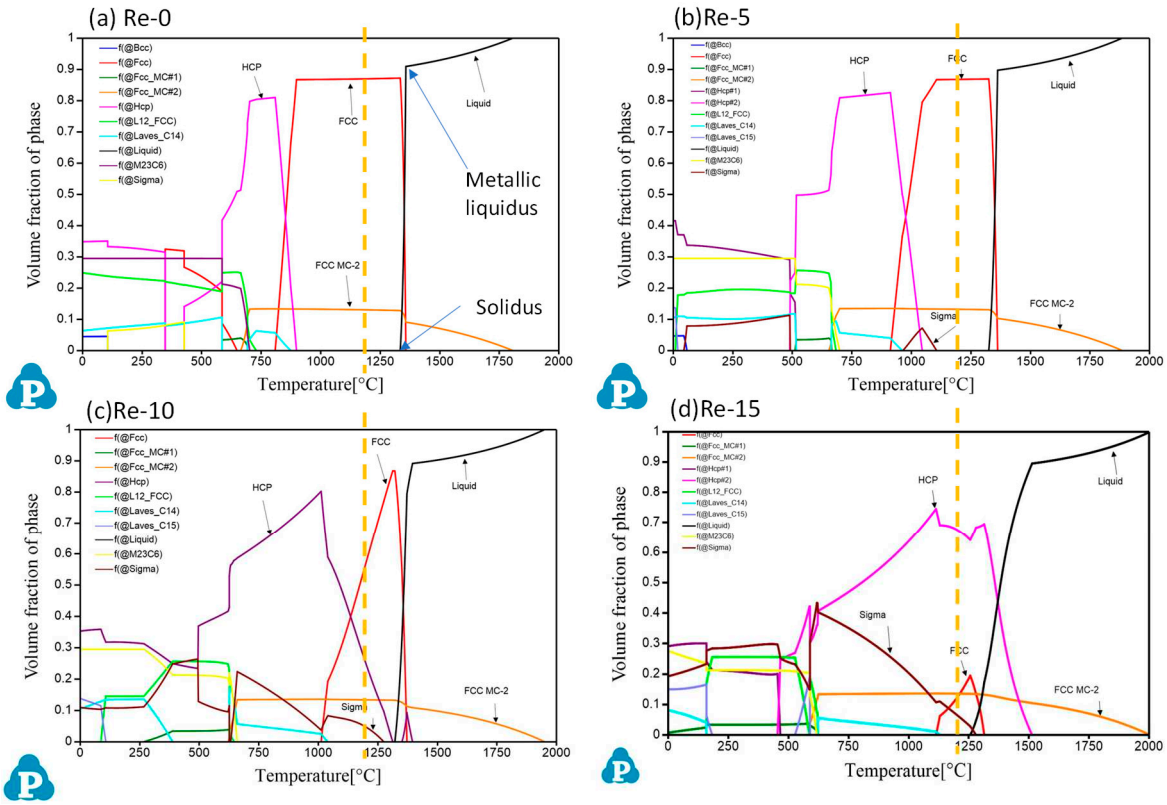

Figure 3. Predicted phase diagrams of (a)Re-0, (b)Re-5, (c)Re-10 and (d)Re-15 derived from Pandat 2020 software with Pan-2020 database. Dashed lines indicate the phase composition at 1200°C.

In contrast, the exothermic change of the sample results in positive heat flow from the sample to the reference, and is therefore shown as a positive peak in the heat flow curve [27]. These changes in the heat flow curves can be used to determine the transition temperatures and the reaction temperatures of the samples.

The beginning of the endothermic peak during the heating stage can be used to estimate the temperature at which melting begins in the Co-Cr-Re-Ta-Ti-C samples, which could be assigned as "solidus temperature". The results show that the solidus points of Re-0, Re-5 and Re-10 are 1295.9°C, 1321.4°C, and 1297.9°C, respectively, suggesting that up to the 10 at% addition of Re does not drastically change the solidus temperature of the alloys investigated, which agreed well with the Pandat predictions. However, the addition of 15 at% Re significantly increased the solidus temperature (1364.3°C).

On the other hand, the onset of the exothermic peak during the cooling phase, derived from the DTA measurement, can be considered as the temperature at which the samples begin to solidify. In the calculated phase diagrams in **Figures 3**, it corresponds to the point where the rapid increase in the volume fraction of the liquid phase abruptly stops, as indicated by the arrow in **Figure 3(a)**. Above this point, all metallic phases melt completely. Hence, the point is referred to as the "metallic liquidus point" in the present study. In the DTA analysis, Re-0 for 1356.8°C, Re-5 for 1361.1°C and Re-10 for 1364°C were assigned as the metallic liquidus points. Again, there is no significant difference between 0 and 10 at% Re. Further addition of Re (15 at%) increased the liquidus temperature to 1389.9°C. **Figure 5(a)** compares the solidus temperatures measured using DTA with the predicted values shown in **Figure 3** to assess the reliability of the prediction software and database. The results from Re-0 to Re-10 show reasonable agreement between the experimental and predicted values, with differences of 38.2°C, 3.4°C and 23.3°C, respectively. The result for sample Re-15, which has the

Preprints (www.preprints.org) | NOT PEER-REVIEWED | Posted: 17 November 2023 doi:10.20944/preprints202311.1123.v1

highest content of Re (15 at%), shows a significant discrepancy, with the predicted temperature being lower than any of the other samples and differing from the experimental results by 108.4°C. Regarding the "metallic liquidus" temperature at which metallic phases are completely melted, the trend is similar for both experimental and predicted results, with the melting temperature increasing with increasing addition of Re **(Figure 5(b))**. It is noteworthy that there is excellent agreement for Re-0 and Re-5 within 1°C of the deviations. However, the difference becomes much larger with increasing Re content; the predicted temperatures are 31.5°C higher than the experimental results for Re-10 and 123.4°C higher for Re-15.

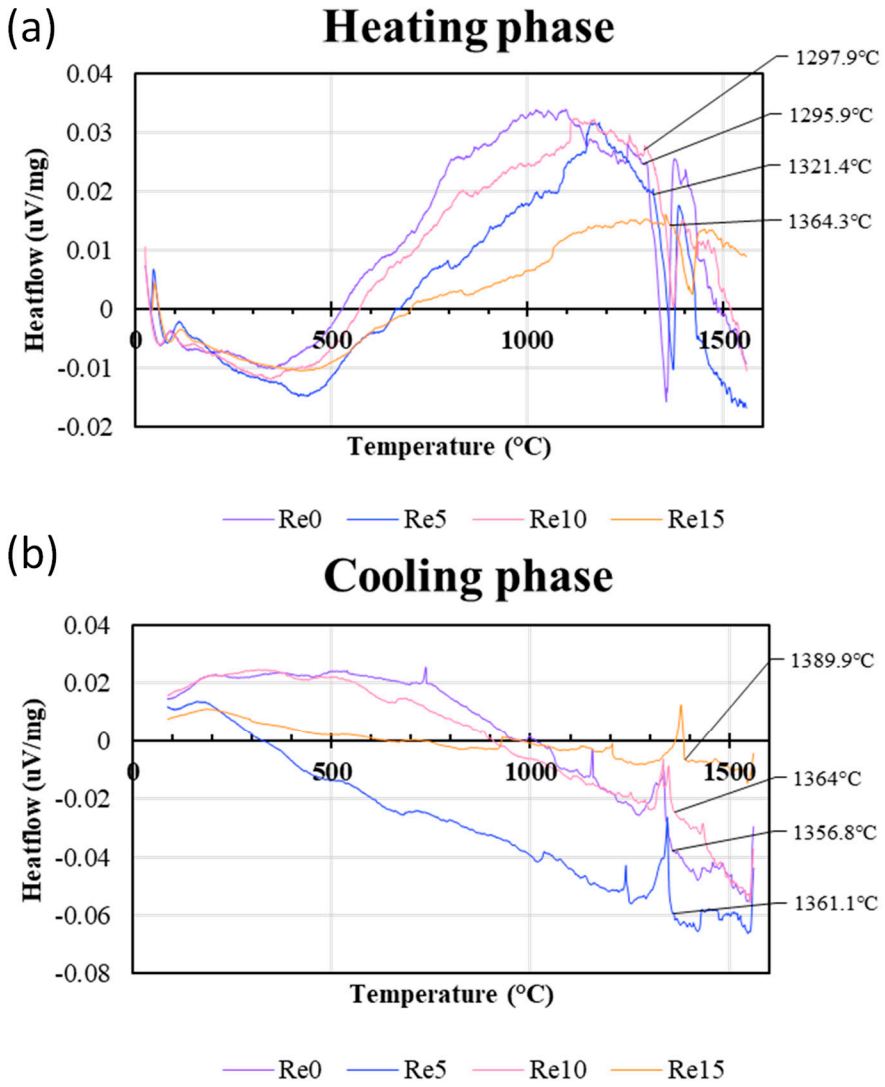

Figure 4. DTA heat flow curves of CoCrReTaTiC alloys: (a) from room temperature to 1550°C, (b) from 1550°C to room temperature.

The comparison showed generally good agreement up to 10 at% Re addition, whereas for Re-15 there was a large gap between the calculated predictions and the experimental results. In particular, the metallic liquidus temperature was estimated to be higher and the solidus temperature was estimated to be lower. In the calculation, the initial solidification of the metallic phase in Re-15 is predicted to be the Re-rich HCP phase, and the lower solidus point is due to the predicted occurrence of eutectic reactions. On the other hand, the microstructural analysis and DTA measurement did not confirm the possible eutectic reactions, suggesting that the Pan-Ni database is not suitable for predicting the phases of the Co-Cr-Ta-Ti-Re-C alloy system when the Re content exceeds 10 at%.

Preprints (www.preprints.org) | NOT PEER-REVIEWED | Posted: 17 November 2023 doi:10.20944/preprints202311.1123.v1

Nevertheless, excellent agreement between Pandat predictions and experimental results was obtained for Re-0 and Re-5, confirming the usefulness of the simulation tool for phase prediction.

Further experiments in the Co-Cr-Ta-Ti-Re-C alloy system could help to improve the accuracy of the predictions, especially for alloys with higher alloying additions such as Ta, Ti and Re.

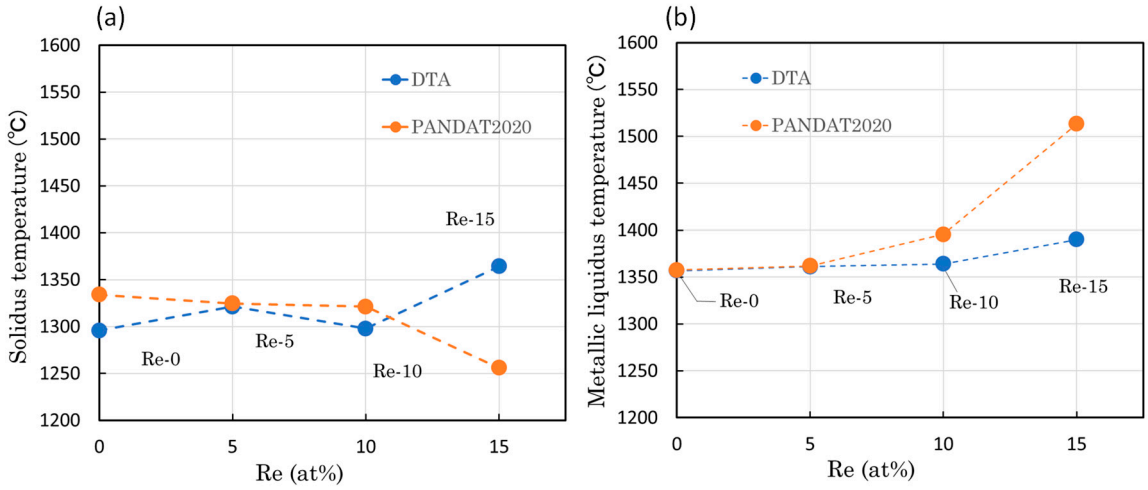

Figure 5. Comparison of melting temperatures experimentally determined by DTA and predicted by Pandat software: (a)solidus temperature and (b)metallic liquidus temperature.

3.3 Oxidation resistance at 1200°C

Figure 6(a) shows the morphological appearance of the samples after 20 hours of air exposure at 1200°C, along with the spalled oxides left on the Al_2O_3 plate (**Figure 6(b)**). The photographs show a blue halo on the alumina plate, indicating that blue oxides, such as Cr-rich oxide, were formed, evaporated and deposited on the alumina plate. It is also likely that Co-rich oxides were melted or spalled and deposited. The alloys, Re-0, Re-5, and Re-10 have similar amounts of spalled oxide in the form of a powder that has spalled from the samples. On the other hand, alloy Re-15 shows a greater amount of spalled oxides in both powder and solid forms. In order to semi-quantitatively compare the oxidation behavior of the samples, the mass change per surface area,, $\Delta m/S$, was estimated, where the surface area "S" is defined as $S = S_{Top\ Surface} + S_{Side\ Surface}$, and the results are summarized in **Figure 6(c).** Note that the sample mass does not include the spalled oxides. **Figure 6(c)** suggests that Re-15 has lost a significant amount of surface oxide through evaporation or spalling, indicating poor oxidation resistance.

Figure 7 shows XRD profiles taken from the top surface of the alloys after 20 hours of oxidation at 1200°C. All the alloys show the presence of two FCC oxide phases, one HCP oxide phase, and one tetragonal oxide phase. The addition of 5 at% Re contributes to the formation of two additional oxide phases: a Cr and Re-rich tetragonal phase and a Re-rich cubic-centered oxide. The peak intensity of the Re-rich oxide appears to increase at 37.05° (corresponding to the (200) diffraction), 72.93° (corresponding to the (321) diffraction), and 127.94° (corresponding to the (440) diffraction). To further identify the oxides formed, cross-sectional analyses were performed using BSE and EDS and are summarized in **Figure 8**. It should be noted that these images were taken from the top surface of the samples placed on the Al_2O_3 plate (see **Figure 6(a)**).

Preprints (www.preprints.org) | NOT PEER-REVIEWED | Posted: 17 November 2023 doi:10.20944/preprints202311.1123.v1

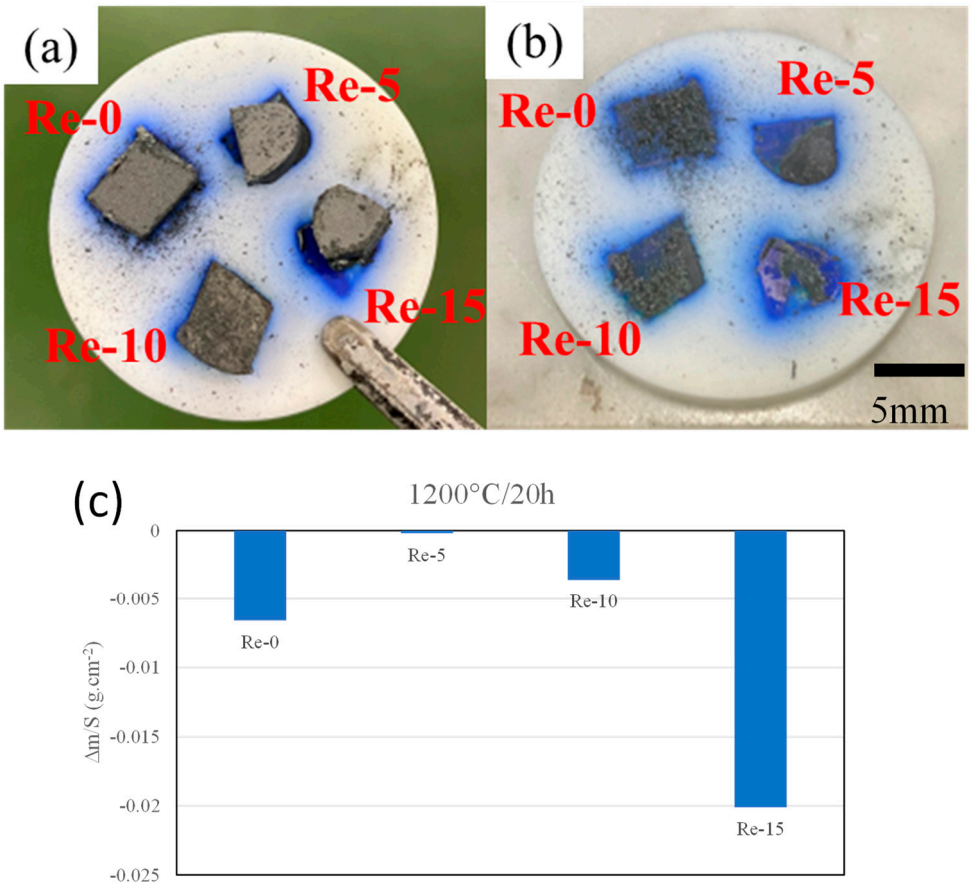

Figure 6. (a) Appearances of the alloys oxidized at 1200°C for 20h followed by air cooling, (b) oxides left from the alumina plate, (c) mass changes of the alloys per exposed surface area.

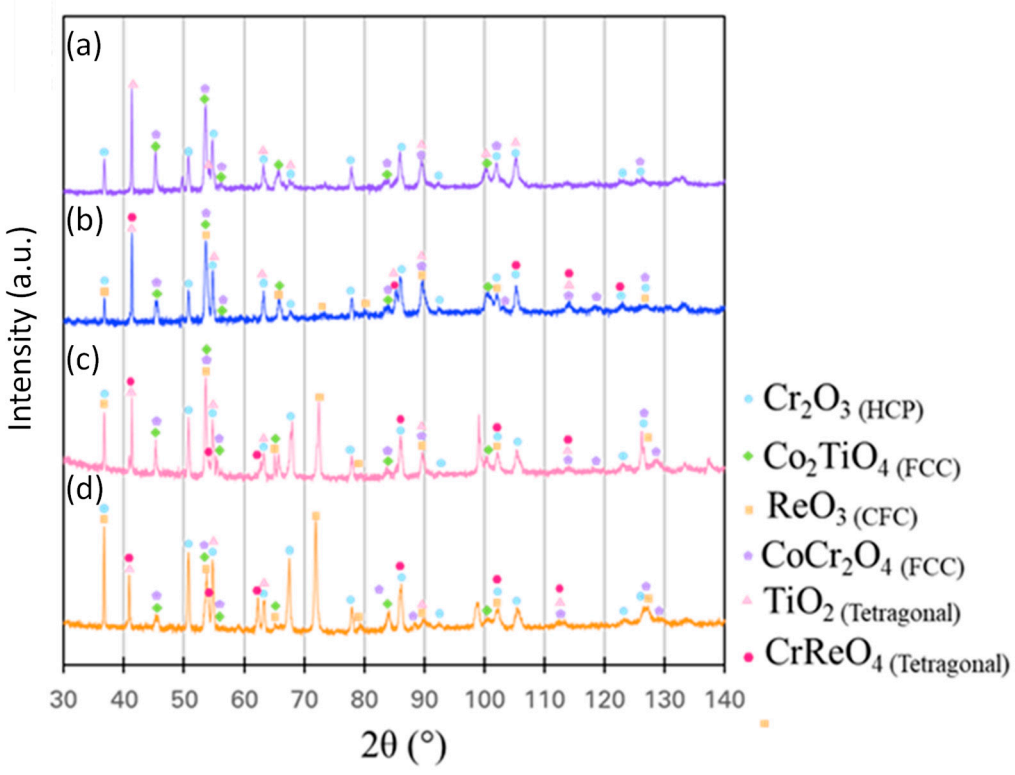

Figure 7. XRD profiles of the surfaces of samples after 20 h of air oxidation at 1200°C. (a) Re-0, (b) Re-5, (c) Re-10 and (d)Re-15. .

 doi:10.20944/preprints202311.1123.v1

The presence of Cr_2O_3 (shown as the green area in the elemental mapping in **Figure 8**) is observed in all alloys, but its volume fraction decreases drastically in Re-15. In addition, internal oxidation seems to be promoted with increasing Re-content, indicating reduced protection against oxidation at 1200°C. For Re-5 and higher, the presence of CoO (shown in orange in **Figure 8**) is observed. This oxide is present above the Cr_2O_3 layer for Re-5, but is mixed with Cr_2O_3 by Re-10. In Re-15, the Co oxide is present both on the top surface and in the Cr, Re and Co mixed oxide layer. As mentioned earlier, the formation of Co oxide is not favorable due to its porous nature and poor oxidation resistance. The formation of porous oxides does little to reduce the oxygen partial pressure beneath this layer, thus suppressing the formation of a continuous protective Cr_2O_3 layer.

The presence of Re appears to facilitate the oxidation of other elements, leading to accelerated internal oxidation and the formation of pores on the surface of the alloys. The Re oxide is volatile [20, 21] and therefore easily evaporates during heat exposure, so the presence of Re oxides (shown in purple with the oxygen enrichment in **Figure 8**) is not easily observed. In addition, the continuous evaporation of Re oxide promotes pore formation, thereby suppressing the formation of dense and continuous surface oxide layers, resulting in accelerated oxidation of other elements. The thinner Cr_2O_3 layer observed in Re-15 could be explained by the accelerated formation and evaporation of non-continuous Cr_2O_3 due to the high rate of Re evaporation. The accelerated oxidation of other elements, such as Co, Ti and Ta, also promotes the spallation of their oxides, as shown in **Figure 6(b)**. Thus, it is concluded that Re-10 and Re-15 suffer from the rapid formation of volatile oxides and their evaporation, together with the formation of other oxides and their spallation, resulting in significant mass loss by the oxidation test. On the other hand, the mass change of Re-5 is the smallest among the alloys studied. However, by comparing the cross-sectional microstructure between Re-0 and Re-5, the thickness of the oxidized region is greater in Re-5, where internal oxidation is also observed. These results suggest that Re-0 and Re-5 have almost identical mass loss caused by vaporization and spallation of oxides, but the remaining oxidized region is larger in Re-5, concluding that 5at% Re addition may not necessarily improve oxidation resistance in this alloy system.

In this study, the addition of Re to the Co-Cr-Ta-Ti-C alloys did not modify the melting temperatures or oxidation resistance. In fact, excessive addition (15at%) drastically worsened the oxidation resistance. However, Re is still an attractive element because it is expected to improve the mechanical properties. [15,16]

One of the solutions to improve the oxidation resistance is to design alloys that could form $CrTaO_4$, as this complex and protective oxide layer has been shown to be stable and effective up to 1200°C [14], whereas no $CrTaO_4$ was observed in all the alloys investigated in this study. Optimization of the Co-Cr-Ti-Ta-C alloy composition with the small addition of Re, using thermodynamic calculation software, would help to develop new alloys with the good combination of mechanical properties and oxidation resistance, which should be investigated in the future.

Preprints (www.preprints.org) | NOT PEER-REVIEWED | Posted: 17 November 2023 doi:10.20944/preprints202311.1123.v1

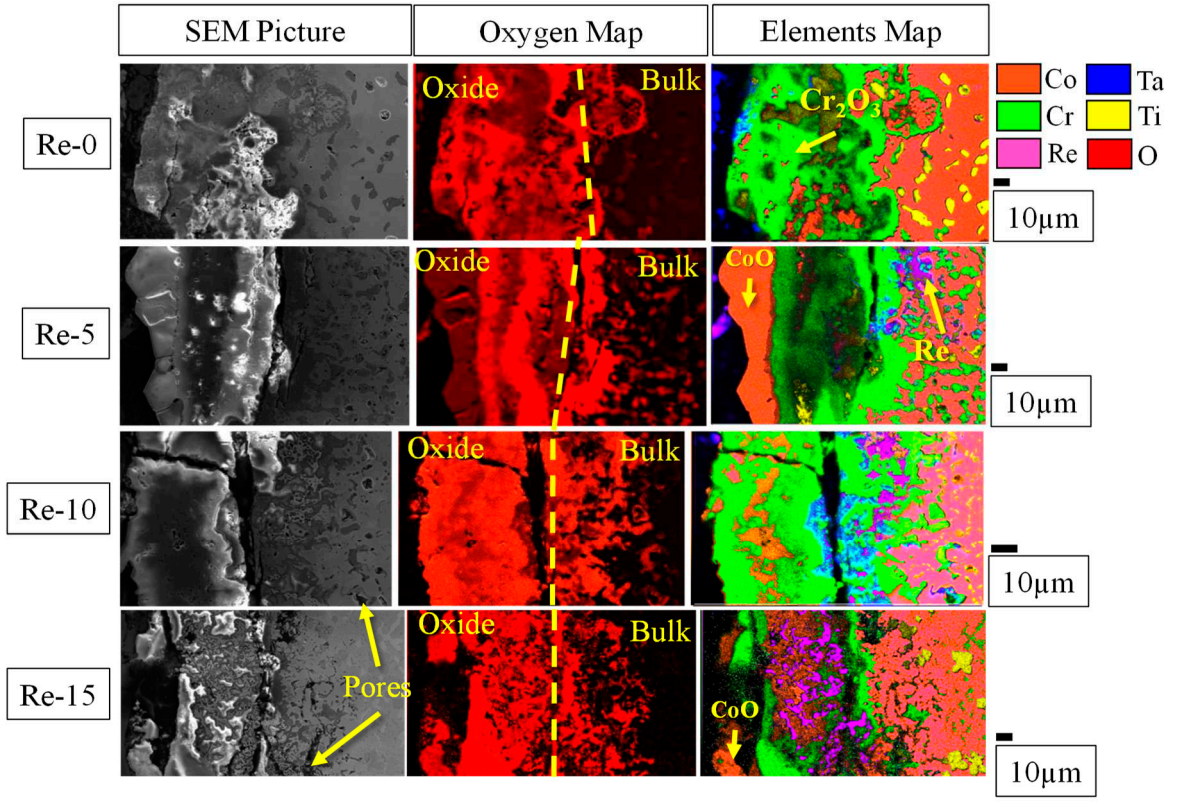

Figure 8. Cross-sectional micrographs of alloys after 20 h of oxidation at 1200°C and corresponding oxygen and elements mapping by EDS.

4. Conclusions

To investigate the effect of Re on the microstructure and oxidation resistance of Co-Cr-Ta-Ti-C alloys, four samples with different levels of Re were investigated. Microstructural characterization revealed that all samples consist of a Co-rich matrix of mixed HCP and FCC phases with $TaTiC_2$ carbides. The addition of Re appears to affect the microstructure from 10 at% due to the formation of the sigma phase. These results were compared with predictions using the Pandat software. This type of software could greatly facilitate the development of new alloys in the future by providing optimal compositions with a reduced number of experiments. The predictions were generally in agreement with the observations, although some differences were observed for alloys with high levels of Re, probably due to the limited number of data with high levels of alloying additions in the PanNi2020 database used for the predictions. The predictions can also be used to estimate the melting temperatures of new alloy compositions, which were compared with the DTA results for the Co-Cr-Re-Ta-Ti-C samples. The results show that the addition of 15 at% Re significantly changes the melting temperature, while the addition of up to 10 at% Re does not change the melting temperatures. In comparison with the predictions made by Pandat, generally good agreement was obtained with the experimental results up to 10 at% Re addition, but there was a large discrepancy for Re-15. Finally, the oxidation resistance of the alloys at 1200°C was tested and showed that increasing the amount of Re had a negative effect on the protection against oxidation, with the formation of a large amount of porous CoO and volatile ReO_3 and an evaporation of protective Cr_2O_3.

In conclusion, the addition of Re does not drastically increase the melting temperatures, which is expected to improve the properties at high temperatures up to 10 at%, but the addition of 15% abruptly modified the melting temperatures. However, this improvement comes at the cost of a deterioration in oxidation resistance with the formation of detrimental oxides and an evaporation of protective Cr_2O_3. This study also demonstrated the potential of predictive software such as Pandat to accurately predict phase constitutions, but the accuracy of the predictions is dependent on the database and the compositional range.

Author Contributions: "Conceptualization, L.M. and H.M.; methodology, L.M. and S.B.; investigation, all the authors.; writing—original draft preparation, L.M.; writing—review and editing, A.I and H.M.; supervision, H.M. All authors have read and agreed to the published version of the manuscript."

Funding: This research received no external funding.

Institutional Review Board Statement: Not applicable.

Informed Consent Statement: Not applicable.

Data Availability Statement: The data of this study are available from the corresponding author upon reasonable request.

Acknowledgments: The authors would like to thank Mr. Po Heng Chou, National Tsing Hua University, Taiwan for assisting the authors with the thermodynamic calculations, and Dr. Takanobu Hiroto, NIMS for XRD analysis. L.M. also acknowledges NIMS Joint Graduate Program for supporting his living expenses.

Conflicts of Interest: The authors declare no conflict of interest.

References

1. Wright, L.G., Gibbons, T.B., Recent developments in gas turbine materials and technology and their implications for syngas firing, *International Journal of Hydrogen Energy*, **2007**, *32*, 3610-3621. https://doi.org/10.1016/j.ijhydene.2006.08.049.
2. Mouritz, A. P., Superalloys for gas turbine engines, Introduction to Aerospace Materials, Woodhead Publishing, 2012, Pages 251-267, ISBN 9781855739468, https://doi.org/10.1533/9780857095152.251.
3. Kirka, M. M., Fernandez-Zelaia, P., Additive Materials for High Temperature Applications, in *Encyclopedia of Materials: Metals and Alloys*, Francisca G. Caballero, Elsevier, 2022, Vol.1, pp529-536. https://doi.org/10.1016/B978-0-12-819726-4.00110-1.
4. Reed, R.C., *The Superalloys, fundamentals and Applications*, Cambridge University Press, The Edinburgh Building, Shaftesbury Road, Cambridge, CB2 2RU, UK, 2006. ISBN 0-521-85904-2.
5. Makineni, S.K., Sharma, A., Pandey, P., Chattopadhyay, K. An Overview on Co-Base Alloys for High Temperature Applications. in *Encyclopedia of Materials: Metals and Alloys*, Francisca G. Caballero, Elsevier, 2022, Vol.1, pp323-334. https://doi.org/10.1016/B978-0-12-803581-8.12094-6.
6. Coutsouradis, D., Davin, A., Lamberigts M., Cobalt-based superalloys for applications in gas turbines, *Materials Science and Engineering* **1987**, *88* 11-19. https://doi.org/10.1016/0025-5416(87)90061-9
7. Berthod, P., Himeur, Z., Panteix, P.J., Influences of the Co content and of the level of high temperature on the microstructure and oxidation of cast {Ni, Co}-based Cr-rich TaC-containing cast alloys, *Journal of Alloys and Compounds*, **2018**, *739*, 447-456, https://doi.org/10.1016/j.jallcom.2017.12.254.
8. Berthod, P., et. al., "REFRACTORY ALLOY, FIBRE-FORMING PLATE AND METHOD FOR PRODUCING MINERAL WOOL", US patent, Patent No. US 8,262,964B2, **2012**.
9. Gu, Y.F., Harada, H., Ro, Y., Chromium and chromium-based alloys: Problems and possibilities for high-temperature service, *JOM*, **2004**, *56*, 28–33. DOI: 10.1007/s11837-004-0197-0.
10. Birks, N.; Meier, G.H.; Pettit, F.S., Introduction to the High. Temperature Oxidation of Metals, 2nd ed.; Cambridge University Press: New York, NY, USA, 2006.
11. Khalid, F.A., Hussain, N., Shahid K.A., Microstructure and morphology of high temperature oxidation in superalloys, *Materials Science and Engineering: A*, **1999**, *265*, 87-94, https://doi.org/10.1016/S0921-5093(98)01181-2.
12. Sahlaoui H., Makhlouf K., Sidhom H., Philibert J., Effects of ageing conditions on the precipitates evolution, chromium depletion and intergranular corrosion susceptibility of AISI 316L: experimental and modeling results, *Materials Science and Engineering: A*, **2004,** *372*, 98-108, DOI: 10.1016/j.msea.2003.12.017.
13. Sahlaoui, H., Sidhom, H., Philibert J., Prediction of chromium depleted-zone evolution during aging of Ni–Cr–Fe alloys, *Acta Materialia*, **2002**, *50*, 1383-1392, https://doi.org/10.1016/S1359-6454(01)00444-X.
14. Moreau, L.E., Gorsse, S., Lambard, G., Murakami H., Microstructure and oxidation behavior of Co–Cr–Ta ternary alloys, *Journal of Alloys and Compounds*, **2023**, *936*, 167968, https://doi.org/10.1016/j.jallcom.2022.167968.
15. Rösler, J., Mukherji, D., Baranski, T., Co-Re-based Alloys: A New Class of High Temperature Materials?, *Advanced Enginering Materials*, **2007**, *9*, 876-881, https://doi.org/10.1002/adem.200700132.

16. Mukherji, D., Strunz, P., Gilles, R., Karge, L., Rösler, J., Current status of Co-Re-based alloys being developed to supplement Ni-based superalloys for ultra-high temperature applications in gas turbines. *Kovove Materialy*, **2015**, *53*, 287-294. https://doi.org/10.4149/km_2015_4_287.
17. Muktinutalapati, N.R., Materials for Gas Turbines – An Overview, in *Advances in Gas Turbine Technology*, Benini E., IntechOpen, **2011**, DOI: 10.5772/20730.
18. Bochenek, K., Węglewski, W., Morgiel, J., Basista, M., Influence of rhenium addition on microstructure, mechanical properties and oxidation resistance of NiAl obtained by powder metallurgy, *Materials Science and Engineering: A*, **2018**, *735*, 121-130, https://doi.org/10.1016/j.msea.2018.08.032.
19. Skoczylas, P., Kaczorowski, M., Preliminary Study of the Rhenium Addition on the Structure and Mechanical Properties of Tungsten Heavy Alloy, *Materials*, **2021**, *14*. 7365. https://doi.org/10.3390/ma14237365.
20. Karge, L., Gilles, R., Mukherji, D., Beran, P., Strunz, P., Hoelzel, M., Rosler J., Beyond Ni-base Superalloys: Influence of Cr Addition on Co-Re base alloys strengthened by nano-sized TaC particles, *Physica B: Physics of Condensed Matter*, **2018,** *551* 1–5, https://doi.org/10.1016/j.physb.2017.11.059.
21. Gorr, B., Trindade, V., Burk, S., Christ, H. J., Klauke, M., Mukherji D., and Rosler, J., Oxidation Behaviour of Model Cobalt-Rhenium Alloys During Short-Term Exposure to Laboratory Air at Elevated Temperature, *Oxidation of Metals*, **2009**, *71,* 157-172, 10.1007/s11085-008-9133-y.
22. Ma S., Ding Q., Wei X., Zhang Z., Bei H., The Effects of Alloying Elements Cr, Al, and Si on Oxidation Behaviors of Ni-Based Superalloys, *Materials* **2022** *15,* 7352. https://doi.org/10.3390/ma15207352
23. Whittle D.P. and Stringer J., Improvements in high temperature oxidation resistance by additions of reactive elements or oxide dispersions. *Philosophical Transactions of the Royal Society A, Mathematical and Physical Sciences* **1980**, *295*, 309–329 http://doi.org/10.1098/rsta.1980.0124.
24. Selvam, J.D.R., Dinaharan, I., Rai R.S., Matrix and Reinforcement Materials for Metal Matrix Composites in *Encyclopedia of Materials: Composites* Editor(s): Dermot Brabazon, Elsevier, **2021**, *Vol. 2*, Pages 615-639, ISBN 9780128197318, https://doi.org/10.1016/B978-0-12-803581-8.11890-9.
25. Nuri Durlu, Titanium carbide based composites for high temperature applications, *Journal of the European Ceramic Society*, **1999**, *19*, 2415-2419, https://doi.org/10.1016/S0955-2219(99)00101-6.
26. Faber, J., Fawcett, T., The Powder Diffraction File: present and future, *Acta Cryst*., **2002**, *B58*, 325-332, https://doi.org/10.1107/S0108768102003312
27. Principle of Differential Thermal Analysis (DTA), https://www.hitachi-hightech.com/global/products/science/tech/ana/thermal/descriptions/dta.html